DC Voltage Droop Control Structures and its Impact on the Interaction Modes in Interconnected AC-HVDC Systems

Thams, Florian; Chatzivasileiadis, Spyros; Eriksson, Robert

Published in:
Proceedings of the 7th Innovative Smart Grid Technologies

Publication date:
2017

Document Version
Peer reviewed version

DC Voltage Droop Control Structures and its Impact on the Interaction Modes in Interconnected AC-HVDC Systems

Florian Thams and Spyros Chatzivasileiadis
Center for Electric Power and Energy (CEE)
Technical University of Denmark
{fltha} / {spchatz} @elektro.dtu.dk

Robert Eriksson
Market and System Development
Svenska kraftnät
robert.eriksson@svk.se

***Abstract*—Different dc voltage droop control structures for future multi-terminal HVDC systems have been proposed in literature. This paper contributes to the evaluation of those structures by an analysis of their impact on the coupling of the interconnected subsystems. In particular, the modes of the systems are classified in different subsets according to the participation of the various subsystems. Those subsets are then evaluated qualitatively and quantitatively indicating which impact the choice of the droop control structure has on the degree of coupling between the connected ac and dc systems respectively the different HVDC converters. The lowest damped interaction modes of the different subsets are analyzed in more detail.**

***Index Terms*—HVDC transmission, Wind energy integration, Control system analysis, State-space methods**

I. Introduction

The increasing interest in renewable energy sources, often built far away from load centers, also raised interest in HVDC technology as enabler for long distance bulk power transmission. In particular, HVDC based on voltage source converter (VSC) is acknowledged as the appropriate technology for grid connection of offshore wind parks far away from the coast. Several advantages, such as the capability to support weak grids and the smaller converter size compared to HVDC based on line-commutated converter (LCC), makes it the preferred technology for this use case. Further, with VSC-HVDC technology enabling multi-terminal HVDC (MT-HVDC) systems, researchers started to think about larger overlay-grids, allowing the interconnection of different asynchronous areas, even a global grid [1]. However, so far only a few multi-terminal VSC-HVDC systems have been built worldwide [2]. Since even on a smaller scale such an MT-HVDC grid would most likely not be built at once but be developed by step-wise integration of already existing on- and offshore interconnectors, this would raise the question of the interoperability of HVDC systems from different vendors using potentially different control structures. Furthermore, such a system could potentially connect widely dispersed parts of the power system and even asynchronous systems demanding a carefully evaluation of potential interactions between converters in order to avoid potential propagation of disturbances between different subsystems.

The little experience with MT-HVDC systems is also the reason for the lacking standardization of the control structure for such grids. In academia and industry it is acknowledged that it is preferable to have a distributed control architecture to make the grid more resilient against the significant impact of any single malfunction. However, while different control schemes have been proposed, it remains unknown which control structure exactly each vendor is using. While one of the preferred options by academia and industry for the control of the grid side converters (GSCs) is dc voltage droop control [3], several alternative droop control schemes have been discussed in technical literature [4]–[19]. The different dc voltage droop control structures (CS) have been categorized and analyzed in terms of their inherent effect on the power transfer capability [15] and in terms of their disturbance attenuation [20]. Further, in [21] the authors analyze interaction modes and their sensitivity to droop gains and dc breaker inductances in a MT-HVDC system. However, to the best knowledge of the authors, there does not exist an analysis of the impact of the various CSs on the interaction modes between different subsystems. Thus, it remains unknown whether the choice of a certain CS results in an unfeasible stronger coupling of subsystems, as for instance the dc and the ac subsystems. In general, it is preferred to have those systems as decoupled as possible to minimize a potential spread of disturbances from one system into the other.

The contributions of this paper include the following: First, an analysis of the quantitative and qualitative coupling between the different subsystems will be provided for two different tunings of the converters, i.e. whether a certain CS imposes a higher degree of coupling reflected by a higher percentage of interaction modes and whether this also influences the damping ratio of the interaction modes. In particular, we will focus on the coupling between the dc and the ac systems and the coupling between the different HVDC converters. We will show how an increased transient response impacts the coupling of the different subsystems. Further, we will discuss

This work is co-funded by the European Unions Seventh Framework Programme for Research, Technological Development and Demonstration under the grant agreement no. 612748 and by the ForskEL-projekt 12264 Best Paths for DK.

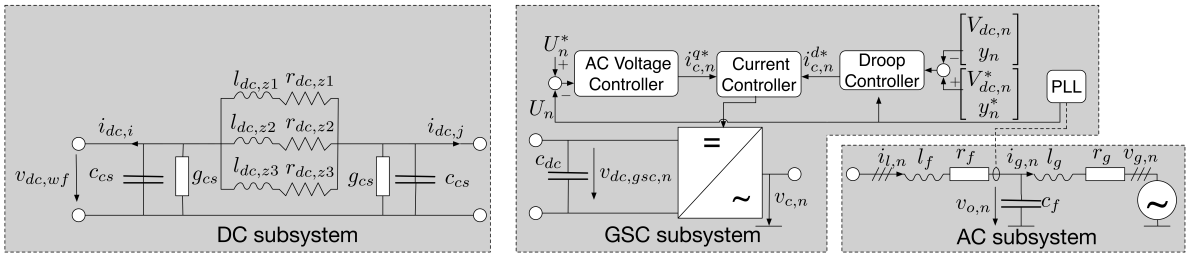

Fig. 1. Splitting of the different subsystems.

how a generalized feedback influences the coupling of those subsystems.

II. Methodology

In [21], the authors propose a methodology to identify and analyze interaction modes between converters in a HVDC system. Here, we adapt the strategy to evaluate how the choice of the CS influences the coupling of the different subsystems:

Given a general linearized model of a HVDC system, which is composed of various subsystems for every connected converter terminal and HVDC cable:

$$\dot{\mathbf{x}} = \mathbf{A}\mathbf{x} + \mathbf{B}\mathbf{u}, \qquad \mathbf{x}(0) = \mathbf{x}_0 \tag{1}$$

with $\mathbf{x} \in R^n$ being the state vector and $\mathbf{u} \in R^m$ the input vector. $\mathbf{A} \in R^n \times R^n$ and $\mathbf{B} \in R^n \times R^m$ are the known coefficient matrices of the steady state linearization around $\mathbf{x_0} \in R^n$.

First, a criterion is defined to distinguish between local modes and interaction modes. Here, interaction modes are defined as modes where at least two subsystems participate. Thus, the participation factors Γ_{ki} measuring the relative participation of the k-th state variable in the i-th mode are determined by:

$$\mathbf{\Gamma} = \{\Gamma_{ki}\} = \{v_{ki} l_{ik}\} \tag{2}$$

where $\mathbf{v}_{ki}$ and $\mathbf{l}_{ki}$ are the k-th entry of the i-th right ($\mathbf{v}_i \in R^{n_t}$) respective left ($\mathbf{l}_i \in R^{n_t}$) eigenvectors of $\mathbf{A}$. Then, $\Gamma_{ki}^n = \frac{\Gamma_{ki}}{\|\mathbf{\Gamma}_i\|}$ are the normalized participation factors. While $\mathbf{\Gamma}_i \in R^{n_t}$ contains the participation factors associated with mode i for all system states, $\|\cdot\|$ denotes the L_1-norm [21]. Further, the vector $\mathbf{\Gamma}_{\alpha,i}^n \in R^{n_\alpha}$ contains all normalized participation factors associated with mode i for all states of the subsystem α.

The overall participation for each subsystem α in mode i is defined as [21]:

$$\eta_{\alpha,i} = \frac{\|\mathbf{\Gamma}_{\alpha,i}^n\|}{\|\mathbf{\Gamma}_i^n\|} \tag{3}$$

with $\|\cdot\|$ denoting the L_1-norm. Focusing on interaction between specific subsystems I^α a set of interaction modes S^α can be defined as:

$$S^\alpha = \{i \mid \eta_{\alpha,i} \geq \chi,\ \forall\, \alpha \in I^\alpha\} \tag{4}$$

with $S^\alpha \subseteq S$, the set of all modes, and χ resembling a threshold chosen as 5% following the example in [21].

Here, two subsets of interaction modes are of particular interest:

- the interaction modes of the subset $S^{ac,dc} = \{i \mid (\eta_{dc,i} \geq \chi) \wedge ((\eta_{ac_1,i} \geq \chi) \vee \cdots \vee (\eta_{ac_N,i} \geq \chi)),\ \forall\ dc, ac_j \in I^{ac,dc}\}$. That means interaction modes with participation of at least one of the connected ac systems and the dc system, since it is preferred to have those systems as decoupled as possible to minimize a potential spread of disturbances from one system into the other.
- the interaction modes of the subset $S^{gsc} = \{i \mid (\eta_{gsc_1,i} \geq \chi) \wedge (\eta_{gsc_2,i} \geq \chi) \wedge \cdots \wedge (\eta_{gsc_N,i} \geq \chi),\ \forall\ gsc_j \in I^{gsc}\}$, i.e. interaction modes between all GSCs, indicating the degree of coupling within the dc grid.

These two subsets will be evaluated quantitatively, i.e. how many of all modes show this type of coupling, and qualitatively, i.e. where are the corresponding eigenvalues located, how critical are they and which states participate in particular?

III. Modeling

The modeling is done according to the generic MT-HVDC model derived in [22]. Each model consists of a number of three different kind of subsystems, shown in Fig. 1.

The ac subsystems are modeled as Thévenin equivalent with an LC-filter interface to the GSCs. Thus, the states corresponding to the ac subsystems, I^{ac_j}, with $j = 1, \ldots, N$, are the following:

$$\mathbf{x}_{ac,j} = \big[i_{g,d,j} \quad i_{g,q,j} \quad v_{o,d,j} \quad v_{o,q,j} \quad i_{l,d,j} \quad i_{l,q,j} \quad v_{o,d,meas,j} \quad v_{o,q,meas,j} \quad i_{l,q,meas,j} \quad P_{ac,meas,j}\big]. \tag{5}$$

Variables $i_{g,d/q,j}$, $i_{l,d/q,j}$ represent the grid current and the line current flowing through the converter. While $v_{o,d/q,j}$ represents the voltage at the point of common coupling (PCC), $v_{o,d/q,meas,j}$ resembles the delayed voltage measurement at the PCC. Further, $P_{ac,meas,j}$ and $i_{l,q,meas,j}$ represent the delayed active power measurement at the PCC and the delayed measurement of q- component of the current flowing though the converter used in the control loops.

The dc grid subsystem includes all dc cables, modelled as 'frequency dependent' π model where the additional parallel RL branches are calculated to fit the frequency response of a wide-band cable model [24], [25]. The model is illustrated in Fig. 1. In general, in a dc grid wind farm side converters (WFC) work as grid forming converter for the connected ac grid without controlling V_{dc}. Hence, due to the focus on the GSC control WFCs can be simplified to dc current sources

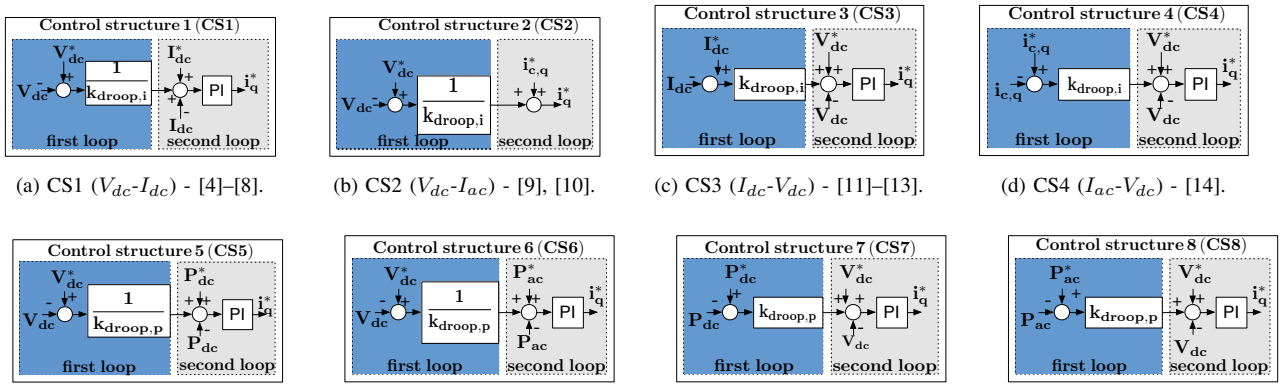

(a) CS1 (V_{dc}-I_{dc}) - [4]–[8]. (b) CS2 (V_{dc}-I_{ac}) - [9], [10]. (c) CS3 (I_{dc}-V_{dc}) - [11]–[13]. (d) CS4 (I_{ac}-V_{dc}) - [14].

(e) CS5 (V_{dc}-P_{dc}) - [16], [17]. (f) CS6 (V_{dc}-P_{ac}) - [23]. (g) CS7 (P_{dc}-V_{dc}) - [18], [19]. (h) CS8 (P_{ac}-V_{dc}) - [19].

Fig. 2. Analyzed dc voltage droop control structures [20].

representing an uncontrolled disturbance for the dc grid [22]. Thus, the states corresponding to the dc subsystem, I^{dc}, are:

$$\mathbf{x}_{dc} = \begin{bmatrix} I_{dc,z(l)} & I_{dc,z(l+1)} & I_{dc,z(l+2)} & \cdots & I_{dc,z(3M-2)} \\ I_{dc,z(3M-1)} & I_{dc,z(3M)} & I_{dc,meas,l} & \cdots & I_{dc,meas,M} \\ & & V_{dc,wf,k} & \cdots & V_{dc,wf,K} \end{bmatrix} \quad (6)$$

with $I_{dc,z(l)}$ - $I_{dc,z(l+2)}$ representing the currents in the different branches of the $l = 1, \cdots, M$ different dc cables. Further, $I_{dc,meas,l}$ represents the delayed dc current measurements at the GSCs, shown in Fig. 1 as $I_{dc,i}$. The variable $V_{dc,wf,k}$ denotes the dc voltage at the $k = 1, \ldots, K$ WFCs.

The GSCs are assumed to be synchronized to the ac grids through a Phase Locked Loop (PLL) and operated with conventional current controllers in the Synchronous Reference Frame (SRF). The current controllers of the GSCs are tuned by the Internal Model Control (IMC) technique designed to track references with a settling time of 10 ms [26]. Saturation limits are included in the control scheme, in order not to exceed the maximum current ratings of the converters.

Both GSCs are assumed to use dc voltage droop control. In general, dc voltage droop control introduces a linear relationship between the dc voltage and a second electric variable, so that the droop gain, k_{droop}, defines the deviation of $V_{dc,j}$ for a variation of the other electric variable:

$$V_{dc,j} = V^*_{dc,j} + k_{droop}(y^*_j - y_j) \quad (7)$$

y^*_j and $V^*_{dc,j}$ are the set points and $V_{dc,j}$, y_j are the measured electric variables respectively. The second electric variable, y_j, can either represent the dc current, $I_{dc,j}$, one component of the ac current, $I_{ac,j}$, the active power measured on the dc side, $P_{dc,j}$, or the active power measured on the ac side, $P_{ac,j}$ [20]. Depending on whether the dc voltage is controlled in the first or the second loop this leads to a total of 8 different dc voltage droop control structures, shown in Fig. 2.

Further, to better control the power sharing between the converters after a converter outage the use of a generalized feedback signal using communication between the GSCs has been proposed [27] as an alternative to the eight CSs using local measurements only. The idea here is, to use a multiple-input feedback controller using all measured voltages deviations as inputs at every terminal, as given in:

$$\begin{bmatrix} \mathbf{\Delta I_{dc,1}} \\ \mathbf{\Delta I_{dc,2}} \\ \vdots \\ \mathbf{\Delta I_{dc,N}} \end{bmatrix} = \begin{bmatrix} g_{11} & g_{12} & \cdots & g_{1N} \\ g_{21} & g_{22} & \cdots & g_{2N} \\ \vdots & \vdots & \ddots & \vdots \\ g_{N1} & g_{N2} & \cdots & g_{NN} \end{bmatrix} \begin{bmatrix} \mathbf{\Delta V_{dc,1}} \\ \mathbf{\Delta V_{dc,2}} \\ \vdots \\ \mathbf{\Delta V_{dc,N}} \end{bmatrix} \quad (8)$$

with g_{xy} corresponding to the inverse of the droop gains, $\frac{1}{k_{droop}}$. Here, however, they are determined by an optimization problem considering the line resistances. Hence, the proposed generalized feedback controller is similar to CS1 (V_{dc}-I_{dc}) but differs by the fact that the generalized feedback controller uses measurements of all GSCs and additional corresponding droop gains.

A comparable performance of power and current based droop control structures and the generalized feedback controller is ensured by the following:

- The droop gains were chosen as $k_{droop,p} = \frac{1}{25}\frac{\text{V}}{\text{kW}}$ as suggested in [22].
- The droop gains used within the power and current based droop controller should be comparable. Thus, the relation derived in [28] is used to determine the current based droop gains, $k_{droop,i_{dc}}$, that are equivalent to the power based droop gains, $k_{droop,p}$:

$$k_{droop,i_{dc}} = \frac{V^*_{dc,j}}{\frac{1}{k_{droop,p}} - I^*_{dc,j}}. \quad (9)$$

  The current based droop gain used for the CSs combining $V_{dc,j}$ and $I_{ac,j}$ needs to be scaled additionally, due to the higher range of $I_{ac,j}$. However, due to the non-linearity of power based droop control, the approximation holds only for a small deviation of the voltage:

$$k_{droop,i_{ac}} = \frac{I^*_{dc,j}}{i^*_{c,q,j}} \cdot k_{droop,i_{dc}}. \quad (10)$$

- For a comparable performance of the generalized feedback control g_{11} and g_{22} are chosen as $\frac{1}{k_{droop,i} - \frac{k_{droop,i}}{2}}$, while g_{12} and g_{21} are chosen as $\frac{1}{k_{droop,i}/2}$.
- Two different for all droop control structures comparable tunings are chosen to show the impact of the tuning on the coupling of the different subsystems. The fast tuning leads

to a fast rise time of approx. $17\,\mathrm{ms}$ and a settling time of approx. $60\,\mathrm{ms}$ with an overshoot of approx. 5%. The slow tuning is reflected by an over-damped response without overshoot, a rise time of approx. $23\,\mathrm{ms}$ and a settling time of approx. $40\,\mathrm{ms}$.

Only the response of CS2(V_{dc}-I_{ac}) differs, due to the absence of a PI controller, since the droop gain already serves as proportional controller connecting $V_{dc,j}$ and $i_{q,j}$ creating the necessary reference variable for the current controller. Hence, the dynamics of CS2(V_{dc}-I_{ac}) are determined by the current controller, which was tuned independently of the outer CS.

Thus, the GSC subsystems, I^{gsc_j}, with $j = 1, \ldots, N$, consist of the following states:

$$\mathbf{x}_{gsc,j} = \begin{bmatrix} pll_{d,j} & pll_{q,j} & \gamma_{d,j} & \gamma_{q,j} & \kappa_{d,j} & \kappa_{q,j} \\ & & V_{dc,j} & V_{dc,meas,j} & P_{dc,meas,j} \end{bmatrix} \quad (11)$$

with $pll_{d/q,j}$ corresponding to the integrator state of the phase-locked loop (PLL). While $\gamma_{d/q,j}$ and $\kappa_{d/q,j}$ represent the integrator states of the current, respective outer controllers, $V_{dc,j}$ and $V_{dc,meas,j}$ represent the dc voltage at the converter and its delayed measurement. Further, $P_{dc,meas,j}$ represents the delayed active power measurement at the GSC.

IV. Case Study

A three terminal grid, shown in Fig. 3, is chosen to evaluate which impact has the choice of the CS on the coupling of the different subsystems. The length of both lines is assumed to be $100\,\mathrm{km}$, parameters are taken from [25]. Choosing the same droop control structure for both GSCs we obtain nine different scenarios (eight different droop CSs, one with generalized feedback). The parameters are given in the appendix. The WFC is assumed to inject maximum power into the HVDC grid with an equal power sharing between the converters. The linearized models are verified by equivalent non-linear models built in Matlab Simulink, which also provide the steady state initial values. As described in the methodology, we focus on two subsets of interaction modes, in particular $S^{ac,dc}$ and S^{gsc}.

A. Subset: AC/DC Interactions

Fig. 4 shows the size of the subset $S^{ac,dc}$ with respect to the set of all modes S in percent in black (fast tuning) and red (slow tuning) respectively. Further, it indicates the minimum damping ratio of the interaction modes in that subset in percent in blue (fast tuning) and green (slow tuning). The first observation is that the coupling of the dc and ac subsystems is affected by the choice of the CS. In fact, depending on the CS and the tuning this subset includes between $11.8\,\%$ (CS7 (P_{dc}-V_{dc}) and CS8 (P_{ac}-V_{dc})) and $21.6\,\%$ (CS6 (V_{dc}-P_{ac}))

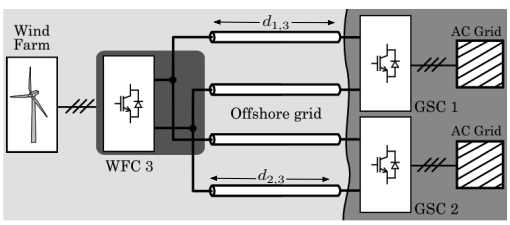

Fig. 3. Three terminal VSC-HVDC grid [22].

of all modes in case of the fast tuning. For the slow tuning it is spread between $0\,\%$ (CS3 (I_{dc}-V_{dc}) and CS7 (P_{dc}-V_{dc})) and $13.7\,\%$ (CS8 (P_{ac}-V_{dc})), considering that there exists no different tuning for (CS2 (V_{dc}-I_{ac}) due to the fact that the CS does not include a PI-controller within the droop controller. Further, unlike it might be intuitively expected the use of an ac measurement within the droop control structure does not necessarily lead to a higher degree of coupling. Further, Fig. 4 also indicates that the damping ratio of the most critical eigenvalue of this subset differs significantly for every CSs as well as for the different tunings (between $16.4\,\%$ (CS6 (V_{dc}-P_{ac})) and $29.3\,\%$ (CS3 (I_{dc}-V_{dc})) for the fast tuning and between $15\,\%$ (CS8 (P_{ac}-V_{dc})) and $100\,\%$ (CS1 (V_{dc}-I_{dc})) for the slow tuning, CS2 (V_{dc}-I_{ac}): $14.8\,\%$). This indicates that not only the degree of coupling of the ac and dc grid depends on the choice and tuning of the CS, but also how well damped disturbances potentially spread between the subsystems.

It is remarkable that for all CSs but CS8 (P_{ac}-V_{dc}) an increased transient response (faster tuning) leads to a higher coupling and lower damping ratio, while it is the other way around for CS8 (P_{ac}-V_{dc}).

The analysis of the participation factors of the lowest damped modes indicates that CSs using the q-component of the ac current within the droop control structure (CS2 (V_{dc}-I_{ac}) and CS4 (I_{ac}-V_{dc})) create a stronger coupling between the outer control loops and therefore for specific modes a stronger coupling between the dc and ac systems. The analysis shows that in this case the subset I^{dc} participates with $\eta_{dc} = 9.4\,\%$ (CS4 (I_{ac}-V_{dc}) (fast tuning)) respectively $\eta_{dc} = 6.9\,\%$ (CS2 (V_{dc}-I_{ac}) in those modes which have a high participation of both ac voltage controllers and corresponding ac states, while in case other CSs are used the dc participation in these modes is $\leq 2.2\,\%$ (fast tuning).

Further, it is worth to mention that both CSs using the dc current (CS1 (V_{dc}-I_{dc}) and CS3 (I_{dc}-V_{dc})) lead to almost complete decoupling of the ac and dc systems in case of the slow tuning, i.e. there exists no (CS3 (I_{dc}-V_{dc})), respectively only very few very well damped eigenvalues. Further, in the fast tuning case, they lead to a medium coupling but all interaction modes are very well damped. In fact, unlike to the other CSs all eigenvalues but two corresponding to the interaction modes have a damping ratio of $100\,\%$ and the

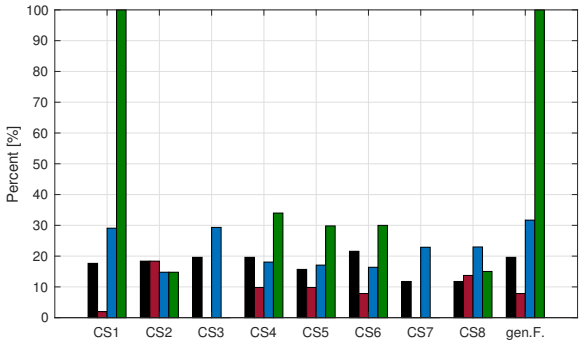

Fig. 4. Size of subset $S^{ac,dc}$ with respect to S in percent for the fast (black) and slow tuning (red). The minimum damping ratio of the corresponding eigenvalues of subset $S^{ac,dc}$ is shown in percent in blue for the fast and in green for the slow tuning.

two remaining ones have significant higher damping ratios ($\geq 29\,\%$) than the lowest damped eigenvalues corresponding to the interaction modes of all remaining CSs.

The impact of the generalized feedback controller can be evaluated by comparing the results of CS1 (V_{dc}-I_{dc}) with the scenario where both GSCs use the generalized feedback controller since they differ only by the use of the measurement signals and additional corresponding droop gains as indicated in III. Figure 4 shows that this leads to a slightly higher number of interaction modes ($21.6\,\%$ to $17.7\,\%$ (fast tuning), $7.8\,\%$ to $2\,\%$ (slow tuning)), hence a higher coupling between the subsystems as intuitively expected due to the communication between the converters. Further, in the fast tuning case, it leads to a slightly higher damping of that aforementioned pair of eigenvalues $31.6\,\%$ to $29.1\,\%$.

Thus, considering that it is preferable to have the ac and dc grid as decoupled as possible with as well damped interaction modes as possible CS7 (P_{dc}-V_{dc}) shows the best properties. For the slow tuning it leads to a complete decoupled system while for the fast tuning it leads to the most decoupled system and a medium damping (together with CS8 (P_{ac}-V_{dc})). Further, CS3 (I_{dc}-V_{dc}) leads to a complete decoupled system with the slow tuning as well. However, in case of the fast tuning a higher coupling of the system (with even though very well damped interaction modes) can be observed. Hence, the best results in particular for the slow tuning are observed for both CSs, combining V_{dc} with dc variables and controlling V_{dc} in the second loop.

On the other hand, CS2 (V_{dc}-I_{ac}) leads to a medium coupling of the systems (size of $S^{ac,dc}$= $18.3\,\%$ of S) and the lowest damping of the most critical interaction mode ($14.8\,\%$). However, considering that TSOs allow damping ratios as low as 3% in their systems, the values of all CSs are not critical in terms of system security. Nevertheless, significant differences between the CSs have been shown.

B. Subset: Converter Interactions

Fig. 5 shows the size of the subset S^{gsc} with respect to the set of all modes S in percent in black (fast tuning) and red (slow tuning) respectively. Further, it indicates the minimum damping ratio of the interaction modes in that subset in percent in blue (fast tuning) and green (slow tuning). The figure shows a high degree of coupling of the two converters and that also the degree of coupling between the different converters depends on the choice of the CS and the tuning, since the size of the subset S^{gsc} varies between $43.1\,\%$ (CS4 (I_{ac}-V_{dc}) and CS6 (V_{dc}-P_{ac})) and $54.9\,\%$ (CS5 (V_{dc}-P_{dc}) and CS7 (P_{dc}-V_{dc})) of S (fast tuning) and between $41.2\,\%$ (CS1 (V_{dc}-I_{dc}) and CS3 (I_{dc}-V_{dc})) and $54.9\,\%$ (CS5 (V_{dc}-P_{dc})) of S. The choice of CS2 (V_{dc}-I_{ac}) leads to $38.8\,\%$ of all modes having a participation of at least $5\,\%$ of both converters.

Further, it is shown that not only the degree of coupling depends on the chosen CS and its damping but also how well those interaction modes are damped. The blue (fast) and green (slow) bars in Fig. 5 indicate minimum damping ratios between $3.3\,\%$ (CS4 (I_{ac}-V_{dc})) and $10\,\%$ (CS6 (V_{dc}-P_{ac})) (fast) and between $10.1\,\%$ (CS7 (P_{dc}-V_{dc})) and $14.3\,\%$ (CS8 (P_{ac}-V_{dc})) (slow), hence significant differences and close to critical damping ratios for CS4 (I_{ac}-V_{dc}). The choice of CS2 (V_{dc}-I_{ac}) leads to a minimum damping ratio of $5.4\,\%$.

Thus, the best performing CS from the previous subset, CS7 (P_{dc}-V_{dc}), leads to a comparably medium (slow) / high (fast) degree of coupling between the GSCs and a comparably low (slow) / medium (fast) level of damping ratio with respect to the other CSs. The second place, CS3 (I_{dc}-V_{dc}), leads to a low (slow) / medium (fast) degree of coupling and comparably low (slow) / medium (fast) damping ratios.

The analysis of the participation factors of the lowest damped modes indicates that all lowest damped modes are related to the outer control loops (mostly ac voltage controllers) and the corresponding ac variables. Thus, the previous observed stronger coupling between the outer control loops in case the q-component of the ac current is used within the droop control structure (CS2 (V_{dc}-I_{ac} and CS4 (I_{ac}-V_{dc}) (fast tuning)) also leads to a lower damping of the most critical interaction modes of the system. However, apart from this and the fact that CSs combining I_{dc} with V_{dc} with a slow tuning lead to a comparably low degree of coupling of the GSCs, there is no clear tendency that a specific combination of variables or order of control loops is better or worse in general within this subsets.

The generalized feedback leads to a higher degree of coupling ($49\,\%$ to $45.1\,\%$) as intuitively expected due to communication between the converters, however, it does not improve the damping of the most critical interaction mode.

C. Discussion

It has been shown that the choice of the CSs as well as the tuning influences the degree of coupling between the different subsystems. Further, a CS leading to a low degree of coupling of dc and ac systems does not consequently also lead to a lower degree of coupling within the dc grid. Additionally, a trade-off between the degree of coupling of the subsystems, the damping of the interaction modes and the response time of the converters was observed.

A CS controlling V_{dc} in the second loop and combining it

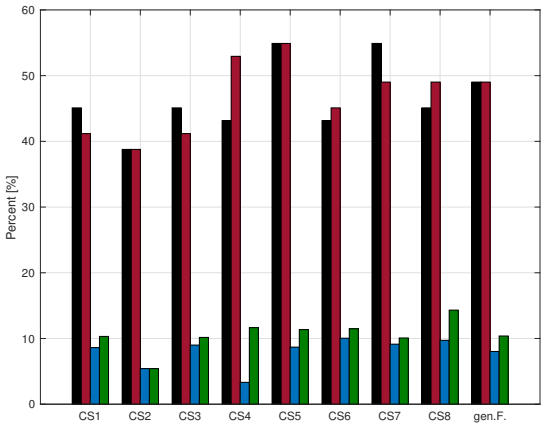

Fig. 5. Size of subset S^{gsc} with respect to S in percent for the fast (black) and slow tuning (red). The minimum damping ratio of the corresponding eigenvalues of subset S^{gsc} is shown in percent in blue for the fast and in green for the slow tuning.

with a second dc variable (I_{dc}/P_{dc}) is in particular with a slow tuning preferable for a decoupling of the dc and ac subsystems. On the other hand, a CS combining V_{dc} with I_{dc} and a slow tuning leads to a comparably low degree of coupling within the dc grid. Thus, CS3 (I_{dc}-V_{dc}) achieves overall the best results with a comparably slow transient response. For a fast response the results are not as clear as for the slow response with different CSs having advantages in different subsets. Considering the higher importance of the subset $S^{ac,dc}$, CS8 (P_{ac}-V_{dc}) is a good candidate for a fast transient response, since it leads to the most decoupled dc and ac subsystems with a comparably medium damping ratio.

Finally, a generalized feedback increases the coupling of the subsystems and the damping of specific but not all interaction modes.

V. Conclusion

This paper presented an analysis of the impact the choice of the droop control structure and its tuning have on the degree of coupling of different subsystems in an interconnected AC/MT-HVDC system. It was shown that the choice of the droop control structure and its tuning influence the degree of coupling of the dc grid with the connected ac grids as well as the degree of coupling between the GSCs. Further, it also influences how well the corresponding interaction modes are damped.

References

[1] S. Chatzivasileiadis, D. Ernst, and G. Andersson, "The Global Grid," *Renewable Energy*, vol. 57, pp. 372–383, 2013.

[2] D. V. Hertem, O. Gomis-Bellmunt, and J. Liang, Eds., *HVDC grids: for offshore and supergrid of the future*. Wiley-IEEE Press, 2016.

[3] V. Akhmatov, M. Callavik, C. M. Franck, S. E. Rye, T. Ahndorf, M. K. Bucher, H. Muller, F. Schettler, and R. Wiget, "Technical guidelines and prestandardization work for first HVDC Grids," *IEEE Transactions on Power Delivery*, vol. 29, no. 1, 2014.

[4] C. D. Barker and R. Whitehouse, "Autonomous converter control in a multi-terminal HVDC system," in *9th IET International Conference on AC and DC Power Transmission*, London, 2010, pp. 1–5.

[5] W. Wang, M. Barnes, and O. Marjanovic, "Droop control modelling and analysis of multi-terminal VSC-HVDC for offshore wind farms," in *10th IET Int. Conf. on AC and DC Power Transmission*, Birmingham, 2012.

[6] O. Gomis-Bellmunt, J. Liang, J. Ekanayake, and N. Jenkins, "Voltage-current characteristics of multiterminal HVDC-VSC for offshore wind farms," *Elec.Power Syst. Research*, vol. 81, no. 2, pp. 440–450, 2011.

[7] L. Xu, L. Yao, and M. Bazargan, "DC grid management of a multi-terminal HVDC transmission system for large offshore wind farms," in *Int. Conf. on Sust. Power Gen. and Supply*, 2009, pp. 1–7.

[8] F. D. Bianchi and O. Gomis-Bellmunt, "Droop control design for multi-terminal VSC-HVDC grids based on LMI optimization," in *50th IEEE Conf. on Decision and Control and Europ. Control Conf.*, Orlando, 2011.

[9] R. T. Pinto, S. Rodrigues, P. Bauer, and J. Pierik, "Operation and control of a multi-terminal DC network," in *IEEE ECCE Asia Downunder*, Melbourne, 2013, pp. 474–480.

[10] Y. Chen, G. Damm, and A. Benchaib, "Multi-Time-Scale Stability Analysis and Design Conditions of a VSC Terminal with DC Voltage Droop Control for HVDC Networks," in *53rd IEEE Conference on Decision and Control*, Los Angeles, CA, 2014.

[11] J. Liang, T. Jing, O. Gomis-Bellmunt, J. Ekanayake, and N. Jenkins, "Operation and Control of Multiterminal HVDC Transmission for Offshore Wind Farms," *IEEE Transactions on Power Delivery*, vol. 26, no. 4, pp. 2596–2604, 2011.

[12] B. K. Johnson, R. H. Lasseter, F. L. Alvarado, and R. Adapa, "Expandable multiterminal dc systems based on voltage droop," *IEEE Transactions on Power Delivery*, vol. 8, no. 4, 1993.

[13] S. Zhou, J. Liang, J. B. Ekanayake, and N. Jenkins, "Control of multi-terminal VSC-HVDC transmission system for offshore wind power generation," in *44th Int. Universities Power Eng. Conf.*, Glasgow, 2009.

[14] F. Thams, J. A. Suul, S. D'Arco, M. Molinas, and F. W. Fuchs, "Stability of DC Voltage Droop Controllers in VSC HVDC Systems," in *PowerTech, Eindhoven 2015*, Eindhoven, 2015.

[15] F. Thams, R. Eriksson, and M. Molinas, "Interaction of Droop Control Structures and its Inherent Effect on the Power Transfer Limits in Multi-terminal VSC-HVDC," *IEEE Transactions on Power Delivery*, vol. 32, no. 1, pp. 182–192, 2017.

[16] P. Rault, F. Colas, X. Guillaud, and S. Nguefeu, "Method for small signal stability analysis of VSC-MTDC grids," in *IEEE Power and Energy Society General Meeting*, San Diego, 2012.

[17] T. M. Haileselassie and K. Uhlen, "Impact of DC Line Voltage Drops on Power Flow of MTDC Using Droop Control," *IEEE Transactions on Power Systems*, vol. 27, no. 3, pp. 1441–1449, 2012.

[18] T. M. Haileselassie and K. Uhlen, "Primary frequency control of remote grids connected by multi-terminal HVDC," in *IEEE Power and Energy Society General Meeting*, Minneapolis, 2010, pp. 1–6.

[19] G. Stamatiou and M. Bongiorno, "Decentralized converter controller for multiterminal HVDC grids," in *15th European Conference on Power Electronics and Applications (EPE)*, 2013, pp. 1–10.

[20] F. Thams, S. Chatzivasileiadis, E. Prieto-Araujo, and R. Eriksson, "Disturbance Attenuation of DC Voltage Droop Control Structures in a Multi-Terminal HVDC Grid," in *PowerTech*, Manchester, 2017.

[21] J. Beerten, S. D Arco, and J. Suul, "Identification and Small-Signal Analysis of Interaction Modes in VSC MTDC Systems," *IEEE Transactions on Power Delivery*, vol. 8977, no. c, pp. 1–1, 2015.

[22] E. Prieto-Araujo, A. Egea-Alvarez, S. F. Fekriasl, and O. Gomis-Bellmunt, "DC voltage droop control design for multi-terminal HVDC systems considering AC and DC grid dynamics," *IEEE Transactions on Power Delivery*, vol. 31, no. 2, pp. 575 – 585, 2015.

[23] T. M. Haileselassie and K. Uhlen, "Precise control of power flow in multiterminal VSC-HVDCs using DC voltage droop control," in *IEEE Power and Energy Society General Meeting*, San Diego, 2012.

[24] J. Beerten, S. D'Arco, and J. A. Suul, "Frequency-dependent cable modelling for small-signal stability analysis of VSC-HVDC systems," *IET Generation, Transmission & Distribution*, vol. 10, no. 6, 2016.

[25] S. Akkari, E. Prieto-Araujo, J. Dai, O. Gomis-Bellmunt, and X. Guillaud, "Impact of the DC cable models on the SVD analysis of a Multi-Terminal HVDC system," in *19th Power Systems Computation Conference (PSCC)*, Genoa, 2016, pp. 1–6.

[26] H. Saad, X. Guillaud, J. Mahseredjian, S. Dennetiere, and S. Nguefeu, "MMC Capacitor Voltage Decoupling and Balancing Controls," *IEEE Transactions on Power Delivery*, vol. 30, no. 2, pp. 704–712, 2014.

[27] J. Beerten, R. Eriksson, D. V. Hertem, and S. Member, "A New Approach to HVDC Grid Voltage Control Based on Generalized State Feedback," pp. 1–5, 2014.

[28] T. K. Vrana, "System Design and Balancing Control of the North Sea Super Grid," Ph.D. dissertation, NTNU, Trondheim, 2013.

[29] T. K. Vrana, Y. Yang, D. Jovcic, S. Dennetière, J. Jardini, and H. Saad, "The CIGRE B4 DC Grid Test System," Cigre, Tech. Rep., 2013.

[30] L. Zhang, "Modeling and control of VSC-HVDC links connected to weak AC systems," Ph.D. dissertation, 2010.

Appendix

TABLE I
PARAMETERS OF THE THREE-TERMINAL DC GRID. CIGRÉ B4 DC GRID TEST SYSTEM [29] AND AC GRIDS [30]

Parameters	Value	Units
GSC/WFC DC link capacitor c_{dc}	150	μF
WFC rated power P_3	700	MW
Reference voltage E^*	400	kV
Nominal power P_1, P_2	350	MW
Nominal voltage V_{ac}	195	kV
Nominal frequency f	50	Hz
Short circuit ratio (SCR)	5	-
Grid Thévenin X_n/R_n ratio	10	-
Coupling inductance L_c	0.2	pu
Coupling resistance R_c	0.01	pu
Capacitor filter impedance X_f	5.88	pu